SANDIA REPORT

SAND2015-8989
Unlimited Release
Printed October 2015

Aerodynamic Design of the National Rotor Testbed

Christopher L. Kelley

Prepared by
Sandia National Laboratories
Albuquerque, New Mexico 87185 and Livermore, California 94550

Sandia National Laboratories is a multi-program laboratory managed and operated by Sandia Corporation, a wholly owned subsidiary of Lockheed Martin Corporation, for the U.S. Department of Energy's National Nuclear Security Administration under contract DE-AC04-94AL85000.

Sandia National Laboratories

Issued by Sandia National Laboratories, operated for the United States Department of Energy by Sandia Corporation.

Available to DOE and DOE contractors from
U.S. Department of Energy
Office of Scientific and Technical Information
P.O. Box 62
Oak Ridge, TN 37831

Telephone: (865) 576-8401
Facsimile: (865) 576-5728
E-Mail: reports@adonis.osti.gov
Online ordering: http://www.osti.gov/bridge

Available to the public from
U.S. Department of Commerce
National Technical Information Service
5285 Port Royal Rd
Springfield, VA 22161

Telephone: (800) 553-6847
Facsimile: (703) 605-6900
E-Mail: orders@ntis.fedworld.gov
Online ordering: http://www.ntis.gov/help/ordermethods.asp?loc=7-4-0#online

SAND2015-8989
Unlimited Release
Printed October 2015

Aerodynamic Design of the National Rotor Testbed

Christopher L. Kelley
Wind Energy Technologies
Sandia National Laboratories
P.O. Box 5800
Albuquerque, NM 87185-1124
clkell@sandia.gov

Abstract

A new wind turbine blade has been designed for the National Rotor Testbed (NRT) project and for future experiments at the Scaled Wind Farm Technology (SWiFT) facility with a specific focus on scaled wakes. This report shows the aerodynamic design of new blades that can produce a wake that has similitude to utility scale blades despite the difference in size and location in the atmospheric boundary layer. Dimensionless quantities circulation, induction, thrust coefficient, and tip-speed-ratio were kept equal between rotor scales in region 2 of operation. The new NRT design matched the aerodynamic quantities of the most common wind turbine in the United States, the GE 1.5sle turbine with 37c model blades. The NRT blade design is presented along with its performance subject to the winds at SWiFT. The design requirements determined by the SWiFT experimental test campaign are shown to be met.

Acknowledgment

This work was performed by Sandia Wind Energy Technologies Department with funding from the Department of Energy Wind and Water Power Technologies Office.

Contents

List of Figures

List of Tables

Nomenclature

a	axial induction factor, $1 - \frac{U}{U_\infty}$
c	blade section chord, m
C_d	drag coefficient
cf	capacity factor
C_l	lift coefficient
$C_{l\alpha}$	lift curve slope
C_m	moment coefficient
C_n	normal force coefficient
C_P	power coefficient
C_T	thrust coefficient
D	rotor diameter, m
h	out of plane blade bending, $h = h_0 \mathrm{e}^{-i\omega_h t}$, m
h_0	amplitude of out of plane blade bending, m
k	shape factor for Weibull distribution
k_1	constant for inverse design chord iteration
k_2	constant for inverse design twist iteration
l	scale factor for Weibull distribution
L	length, m
P	power, W
Q	rotor torque, Nm
r	radial distance from axis of rotation, m
R	radius of rotor swept area, m
Re	Reynolds number
t^*	dimensionless time, tU_∞/R
T	thrust, N
TI	turbulence intensity
u_i	three coordinates component of fluid velocity, m/s
U	axial component of fluid velocity, m/s
U_∞	freestream velocity, m/s
V	ground normal component of fluid velocity, m/s
W	relative velocity seen by airfoil, m/s
x	axial coordinate, m
x_{pa}	distance aerodynamic center is behind pitch axis, m
y	transverse coordinate, m
z	ground normal coordinate, m

α	blade section angle of attack, degrees
β	blade section twist, degrees
Γ	bound circulation along blade span, m^2/s
Γ_s	shed spanwise circulation, m^2/s

Γ_t	shed trailing circulation, m^2/s
Γ'	dimensionless bound circulation along blade span, $\frac{\Gamma}{U_\infty R}$
λ	tip speed ratio, $\frac{\Omega R}{U_\infty}$
ν	kinematic viscosity, m^2/s
ϕ	inflow angle at blade section relative to plane of rotation $\alpha+\beta$, degrees
ρ	air density, kg/m^3
σ	rotor solidity
τ^*	dimensionless shear, $\frac{d\frac{U_\infty}{U_{\infty hub}}}{d\frac{z}{D}}$
ω_h	angular velocity out of plane blade bending, rad/s
Ω	angular velocity of rotor, rad/s

AEP	annual energy production, GWh
fs	full-scale
NRT	National Rotor Testbed
OEM	original equipment manufacturer
Pr()	probability of event
R2	region 2 operation, $\Omega \propto U_\infty$
R2.5	region 2.5 operation, $\Omega = \Omega_{max}$, $P <$ rated
R3	region 3 operation, $\Omega = \Omega_{max}$, $P =$ rated
RMSE	root mean squared error
ss	subscale
SWiFT	Scaled Wind Farm Technology
UTC	Coordinated Universal Time
V27	OEM, Vestas 27 m diameter wind turbine
∞	freestream value

Chapter 1

Motivation

A goal of the National Rotor Testbed project at Sandia is to design a subscale wind turbine blade that has wake similitude to a modern, commercial size blade. Generating a scaled wake would allow for testing of new technologies at less cost than using full-scale wind turbine test facilities. For example, intentional yaw error to vector the wake or active flow control technologies and their impact on wakes and downstream turbines could be investigated at the inexpensive, small scale, knowing that the effects on the wake would scale according to process documented in this paper. A scaled wake should have equal instantaneous dimensionless velocity vectors, u_i/U_∞, at the same spatial positions, x/R, y/R, and z/R at any time, t^* which do not depend on the size of the wind turbine.

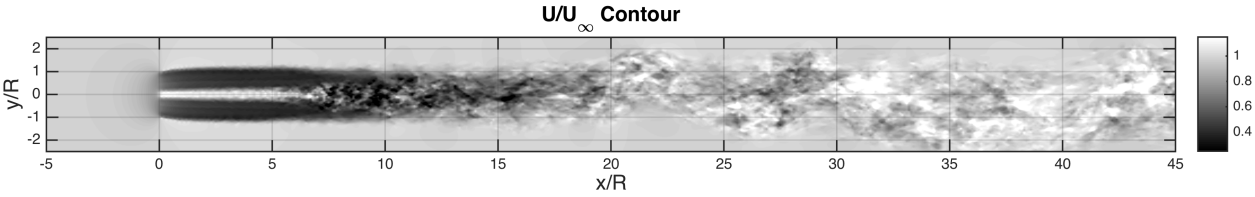

Figure 1.1. A scaled wake should have equal instantaneous velocities, U/U_∞, at the same spatial positions, x/R, y/R at any time, t^*.

A scaled wake is shown in Figure 1.1. The rotor spins in the y–z plane with the center of the hub at (0,0). In the contour, the axial velocity has been normalized by the freestream velocity, and the horizontal and vertical coordinates have been normalized by the rotor radius. There is a near-wake region where the velocity deficit is identical to the blade load distribution extending to approximately 7 rotor radii downstream. Tip vortices begin pairing, forming large coherent structures in the mid-wake, bringing high momentum fluid towards the axis of rotation ($y/R = 0$). In the far wake momentum recovers, coherent structures break apart to finer scales, and the wake meanders at a low frequency. These are the types of flow features and physics that should occur at the same normalized positions with the same dimensionless frequencies for scaled wakes with similarity.

Creating a scaled wake reduces the cost of experiment and can have results applicable to any absolute size. This motivating factor necessitates the following work: a design process

that produces the scaled wake identical to the full-scale wind turbine and an understanding of which dimensionless quantities cannot be held constant and are least important to studying wind turbine wakes and turbine-turbine interaction from an aerodynamic perspective. Similitude is the focus of Chapter 2. Chapter 3 describes how wakes are created by wind turbine blades. The theory of vortex methods is critical to this chapter in relating the bound circulation of the blade to the creation of the turbine wake. Next, Chapter 4 deals with the issue of a scaled wake sitting lower in the same atmospheric boundary layer with meteorological tower analysis at the SWiFT site. Chapter 5 discusses further considerations important to the specific aerodynamic design of a blade at SWiFT and reviews the selected airfoils, how airfoil polar data are interpolated, and how to fully constrain the circulation matching method. Chapter 6 shows how the blade tip was designed with different constraints outboard of 97% blade span. Next, the focus of Chapter 7 is on the creation of an inverse blade design tool that can find the geometry necessary to create a specific scaled wake. Chapter 8 summarizes the performance of the new blade design, including power and blade pitch schedule as a function of wind speed. Chapter 9 includes span location specific parameters for various wind speeds such as lift and drag coefficients, and how the target circulation changes outside of region 2. Chapter 10 shows how blade sweep affects the blade torsion towards feathering. Finally, Chapter 11 reviews how the high level aerodynamic design requirements are met as required by the project planning.

Chapter 2

Problems with Similitude

Testing subscale models and having similarity is fundamental to scaled experiments in fluid dynamics and aerodynamics. If geometric, kinematic, and dynamic similarity are all equal for the model and full-scale, the results of the model are equivalent to testing at full-scale.

Consider first scaling the full-scale wind turbine geometrically. This would ensure geometric similarity. For the present work, an existing tower and generator are available at the SWiFT Facility, therefore the subscale rotor must be nearly 3 times smaller than the commercial full-scale rotor, that is the rotor diameters and chords are in the ratio $c_{fs}/c_{ss} = D_{fs}/D_{ss} = 2.85$ as seen in Figure 2.1.

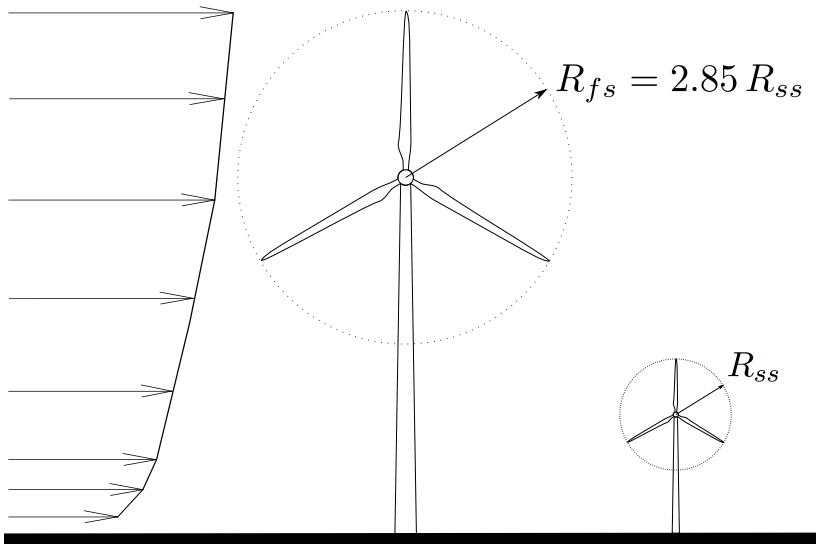

Figure 2.1. Find subscale geometry to produce identical scaled wake to full-scale wind turbine.

The height differences seen between these two rotors change the freestream velocity seen by each rotor. Using the meteorological data at SWiFT, $U_{\infty_{fs}} = 8.6$ m/s and $U_{\infty_{ss}} = 6.8$ m/s. Kinematic similarity ensures that the streamlines of fluid motion are oriented in the same direction, and that the time rates of change of motion are equal. For wind turbines, this important parameter is the tip-speed-ratio, λ. By keeping λ equal for the model and full-

scale, the wake helix angles are equal, and the motion of the blades see equal air velocity relative to the freestream. So to ensure kinematic similarity, $\lambda_{fs} = \lambda_{ss} \therefore \Omega_{ss} = 2.3\Omega_{fs}$. This means that the subscale wind turbine must spin two and three-tenths times faster than the full-scale, and this is achievable at SWiFT.

The last issue is dynamic similarity, the ratio of forces between model and full-scale acting on the turbine blades being constant. At the blade surface this means equal spatial distributions of a dimensionless force coefficients, C_l, C_d, axial induction, a, or circulation, Γ'. And in the fluid motion, the Reynolds numbers should be equal so that range of scales of turbulent motions are identical and dissipating energy at the same rate. Of course, the Reynolds numbers also affects the lift and drag coefficients. The chord Reynolds number as seen by an airfoil section on the blade is

$$Re = \frac{Wc}{\nu} \approx \frac{U_\infty \frac{r}{R} \lambda c}{\nu}. \tag{2.1}$$

In addition the air at atmospheric conditions will have equal kinematic viscosities, ν. And the Reynolds number should be equal at each blade station, r/R.

$$\left(\frac{U_\infty \frac{r}{R} \lambda c}{\nu}\right)_{fs} \stackrel{?}{=} \left(\frac{U_\infty \frac{r}{R} \lambda c}{\nu}\right)_{ss} \quad \therefore 3.6 \neq 1 \tag{2.2}$$

This means that dynamic similarity with respect to Reynolds number cannot be maintained when designing a subscale wind turbine for the same wind speed as a full-scale turbine. A factor of 3.6 in Reynolds number can have a large effect on airfoil performance. However, the spatial distribution of lift or drag coefficients could be equal. If Reynolds number is not important to the wake mixing and dissipation, dynamic similarity of one force could still be achieved by keeping the ratio of lift forces distributed along the blades equal. Previous work has shown that the spatial distribution of dimensionless lift per unit span, Γ', can greatly change the wake structure in uniform and sheared flow conditions, and may be more important to the wake structure than the ratio of inertial to viscous forces. [1, 2]

If the Reynolds number constraint has been relaxed, it may be advantageous to choose new airfoils altogether that perform more efficiently at the three and a half times smaller Reynolds numbers expected for the subscale wind turbine. And this is central to the proposed aerodynamic scaling philosophy, give up geometric similarity, but maintain kinematic similarity by operating in region 2 with the same tip-speed-ratio, and loosely maintain dynamic similarity by keeping the dimensionless circulation equal between the two scales of wind turbines.

Chapter 3

Importance of Circulation to the Wake

Vortex methods have been of great importance to rotor-craft and wind turbine research because they are able to predict the flow field everywhere due to a spinning rotor, and can produce solutions with far less computational cost than CFD. They work based on Kelvin's Circulation Theorem and Prandtl Lifting Line Theory. For greater detail on the theory and computational algorithm see [3, 4, 5]. To highlight, the following computations are involved at every time step of the solution.

- The net circulation bound on the rotor and contained in the wake never changes. $\frac{D\Gamma}{Dt} = 0$
- Spanwise circulation is shed that is proportional to the time rate of change of bound circulation on the blade. $\Gamma_s \propto \frac{d\Gamma}{dt}$
- Trailing circulation is shed that is proportional the the spanwise gradient of bound circulation. $\Gamma_t \propto \frac{d\Gamma}{dy}$
- The Biot-Savart Law is used to calculate induced velocity, W, and inflow angles at all blade stations.
- This information allows for calculation of lift and drag forces, and then torque and power through integration of blade forces.
- The bound circulation is updated for the next time step according to Kutta-Joukowski Theorem. $\Gamma'(t + \Delta t) = \frac{C_l}{2} \frac{W}{U_\infty} \frac{c}{R}$
- All vortex lattice elements in the wake are convected due to Biot-Savart Law.
- Rotate the rotor a small angle.

As seen in the computational steps, bound circulation is key to determining what happens downstream in the wake. At every blade station the local spatial and temporal derivatives of bound circulation determine precisely the circulation introduced at the trailing edge of the

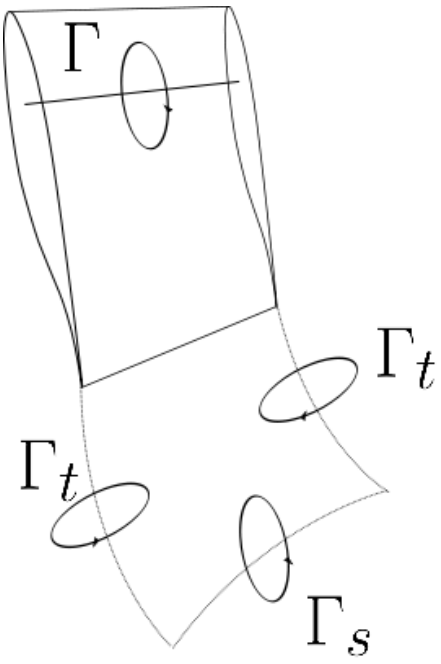

Figure 3.1. Shed circulation is determined by local spatial and temporal derivatives of bound circulation.

blade as seen in Figure 3.1. The trailing vortices are like wingtip vortices due to differences in bound circulation along the blade span. The spanwise vortices are up/downwash motions due to time rate of change of local circulation. This theory highlights the fact that the local slope of bound circulation directly influences the wake of a wind turbine. This is why dimensionless circulation, rather than drag coefficient, has been chosen to be equal in the scaled wake wind turbine design.

Chapter 4

Atmospheric Boundary Layer

The full-scale wind turbine wake that is being reduced in scale will sit lower in the atmosphere, and for a given site location this means different average wind conditions. This chapter highlights how the typical shear and turbulence intensities affect when a scaled wake can be created with some meteorological site analysis at SWiFT.

Figure 4.1 shows the mean wind speed from the ground up to 200 m. This data were collected at the SWiFT site from July 2012 through January 2015 on the Texas Tech 200 m meteorological tower. The subscale wind turbine designed sits 32.1 m above the ground, whereas a utility scale turbine is at 80 m. The mean wind speed for all data recorded

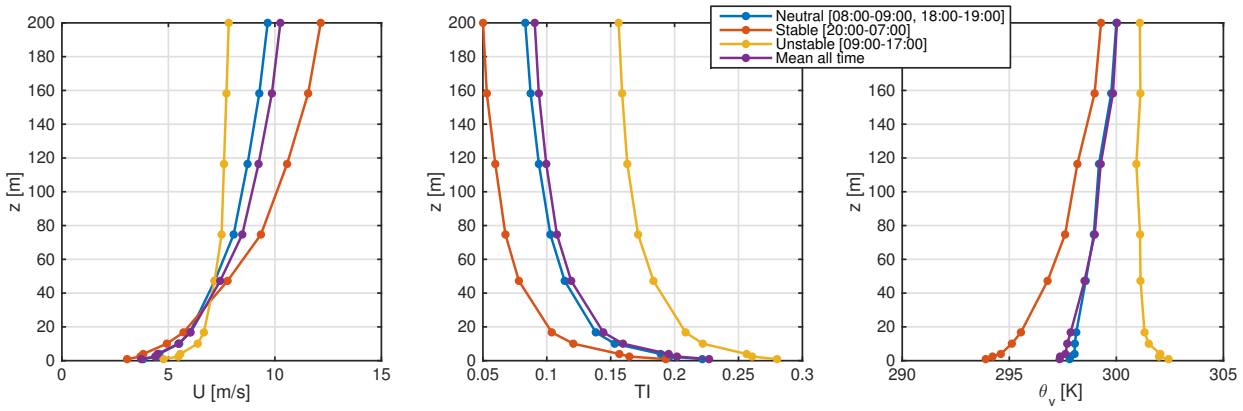

Figure 4.1. Comparing 32.1 m to 80 m hub heights.

showed 6.8 m/s and 8.6 m/s at the subscale and full-scale hub heights respectively. There is also a slope difference, and hence shear, across the two different rotors. The dimensionless shear was found for each as the difference in velocity as a percent of hub height velocity from the top and bottom of the rotor per diameter length. Dimensionless wind shear has been defined as

$$\tau^* = \frac{d\frac{U_\infty}{U_{\infty hub}}}{d\frac{z}{D}}. \tag{4.1}$$

These results are summarized in Table 4.1. On average, the mean wind speed is reduced by 18.5% of the hub height wind speed from top to bottom of the subscale diameter and 23.3%

for the full-scale diameter. The turbulence intensity is also shown as a function of altitude. On average, the subscale and full-scale turbines see 13.0% and 10.5% turbulence intensities respectively at hub height.

Table 4.1. COMPARING SUBSCALE AND FULL-SCALE TURBINES AT SAME WIND SITE

D [m]	P [MW]	z_{hub} [m]	$U_{\infty hub}$ [m/s]	τ^*	TI
27	0.250	32.1	6.81	0.185	0.130
77	1.5	80	8.59	0.233	0.105

Just because the average wind speeds and turbulence for all time are not equal for the different turbine sizes, similar shear and turbulence can be observed at certain times of the day. Diurnal weather patterns due to heating of the ground are known the produce greater turbulence and mixing during the afternoon, and stable, higher shear winds at night. Figure 4.2 averages all hours of the wind data to the average day using Central Standard Time, UTC-06:00. For example, all 10-minute samples falling between 01:00–02:00 are averaged together as 01:00. This provides a glimpse of the average day.

To have equal wind shear at the two scales, testing typically should be done between 11:00 and 20:00 local time, which corresponds to an unstable atmospheric boundary layer from 11:00–17:00 and 19:00–20:00, and neutral from 18:00–19:00. Turbulence intensity for the subscale design is consistently 2.5% higher than the full-scale turbine at all hours of the day. However, these again are averages over 2.5 years. Therefore there will certainly be times where the shear and turbulence closer to the ground are equal to the average shear and turbulence at higher hub heights. However data cannot be collected as quickly until these events occur.

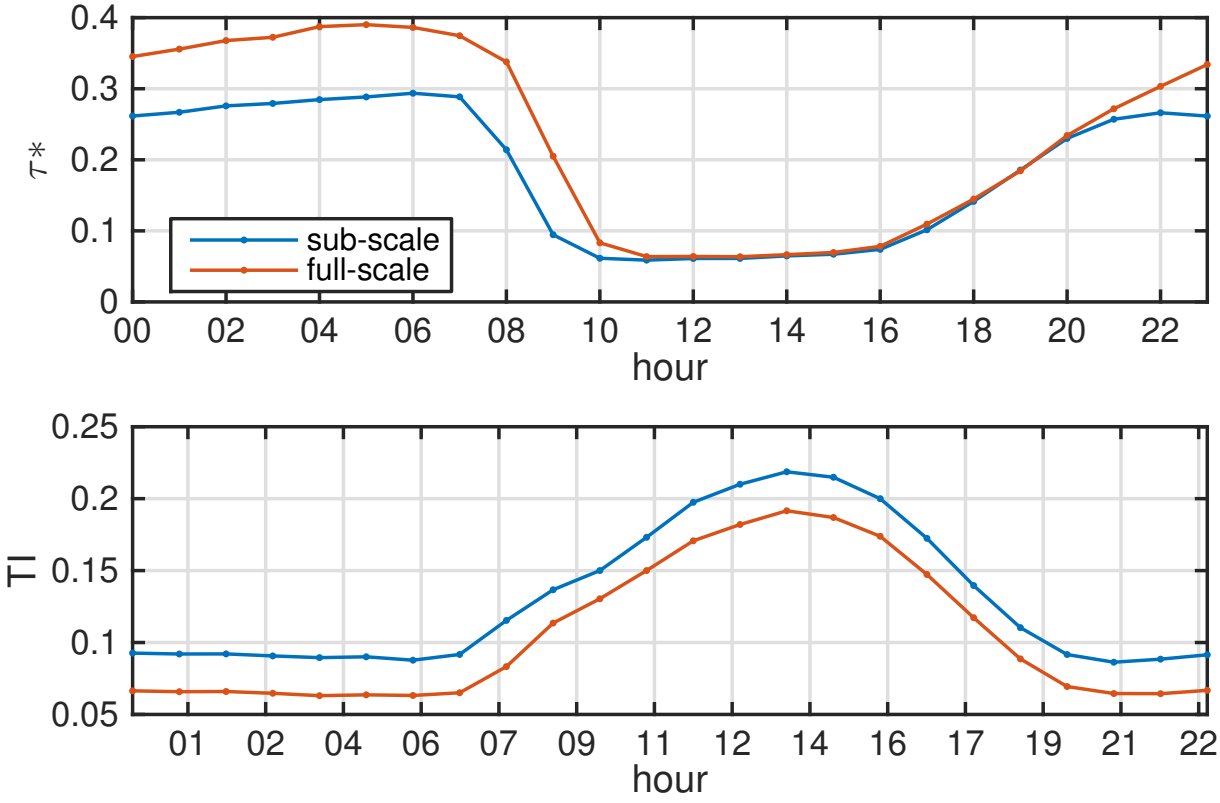

Figure 4.2. Differences in shear and turbulence with turbine size.

Chapter 5

Aerodynamic Design

This chapter discusses a new inverse wind turbine blade design tool that has been implemented which uses a target, dimensionless circulation distribution from a full-scale 1.5 MW wind turbine blade to find the geometry of a new subscale blade that will be manufactured and flown at Sandia's SWiFT facility. In addition, airfoil polar data are interpolated from a few specified span stations leading to a smooth blade that can be manufactured. The iterative process perturbs chord and twist, after running a blade element momentum theory code, to reduce the residual sum of the squares error between the modeled subscale circulation and the target full-scale circulation. Based on the previous scaling issues explained in Chapter 2, geometric similarity has been given up in the hopes of maintaining a similar wake in the new subscale blade design by matching the dimensionless circulation distribution spatially along the blade. This dimensionless circulation Γ' is defined as follows based on the Kutta-Joukowski theorem.

$$\Gamma'\left(\frac{r}{R}\right) = \frac{\Gamma(\frac{r}{R})}{RU_\infty} = \frac{C_l}{2}\frac{W}{U_\infty}\frac{c}{R} \tag{5.1}$$

Geometry and Reynolds number will not be held constant. This necessitates a new inverse design tool which can use different airfoils to find the required blade geometry that will make the subscale blade design have the same bound, dimensionless circulation as the full-scale blade at every dimensionless radial station, r/R. However, just matching circulation does not fully constrain the problem, because many combinations of chord and C_l can produce the same Γ'. Therefore, angle of attack or lift coefficient should also be chosen for the subscale blade design. Having equal C_l for model and full-scale would enforce a specific angle of attack. This is not ideal since the subscale model is using different airfoils which have different stall and maximum efficiency characteristics. A lift coefficient for the subscale design was chosen to be constant, $C_l = 0.6$. This was done to keep the blade fairly close to but below the maximum lift-to-drag ratio, and also keep the blade chord large because lift coefficient decreased near the tip. This created a higher solidity tip required for the blade-interior instrumentation of the National Rotor Testbed experimental campaign.

The new blade will operate at a tip-speed-ratio of 9 and around a maximum Reynolds number of 2.5×10^6 for the average site wind speed. Two S-Series airfoils were chosen which have good aerodynamic characteristics at this Reynolds number, S814 and S825, seen in Figures 5.1 and 5.2 The are insensitive to roughness, have high quality experimental data, and were even tested with harmonic pitching. The experimental airfoil polars for a range of Reynolds numbers are plotted in Figure 5.3 designed and tested by Somers [6, 7].

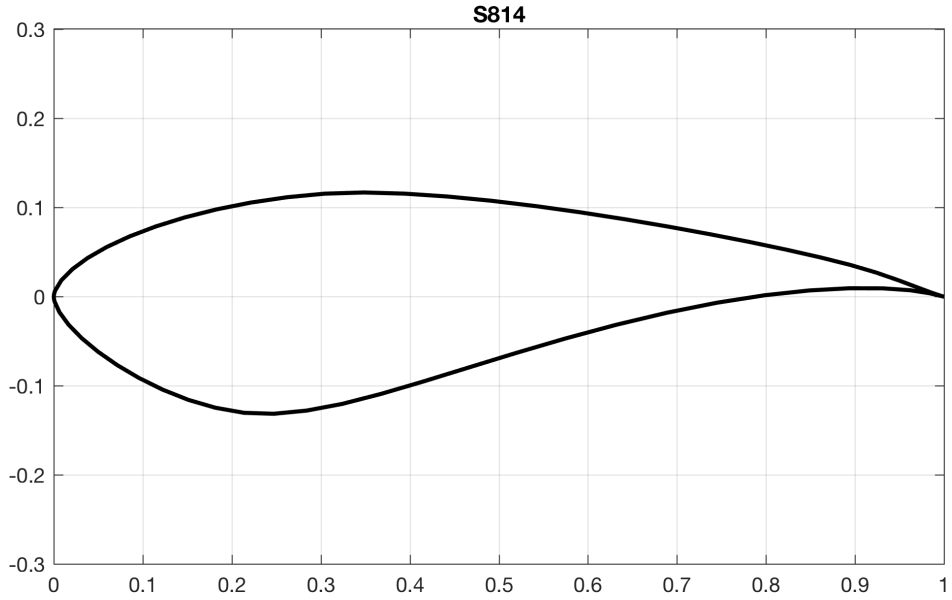

Figure 5.1. S814 airfoil section shape

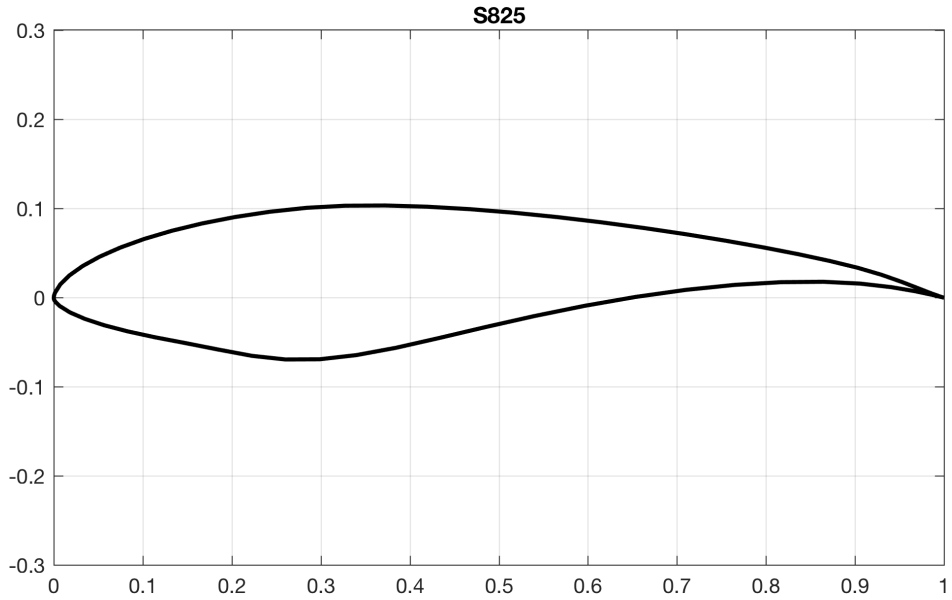

Figure 5.2. S825 airfoil section shape

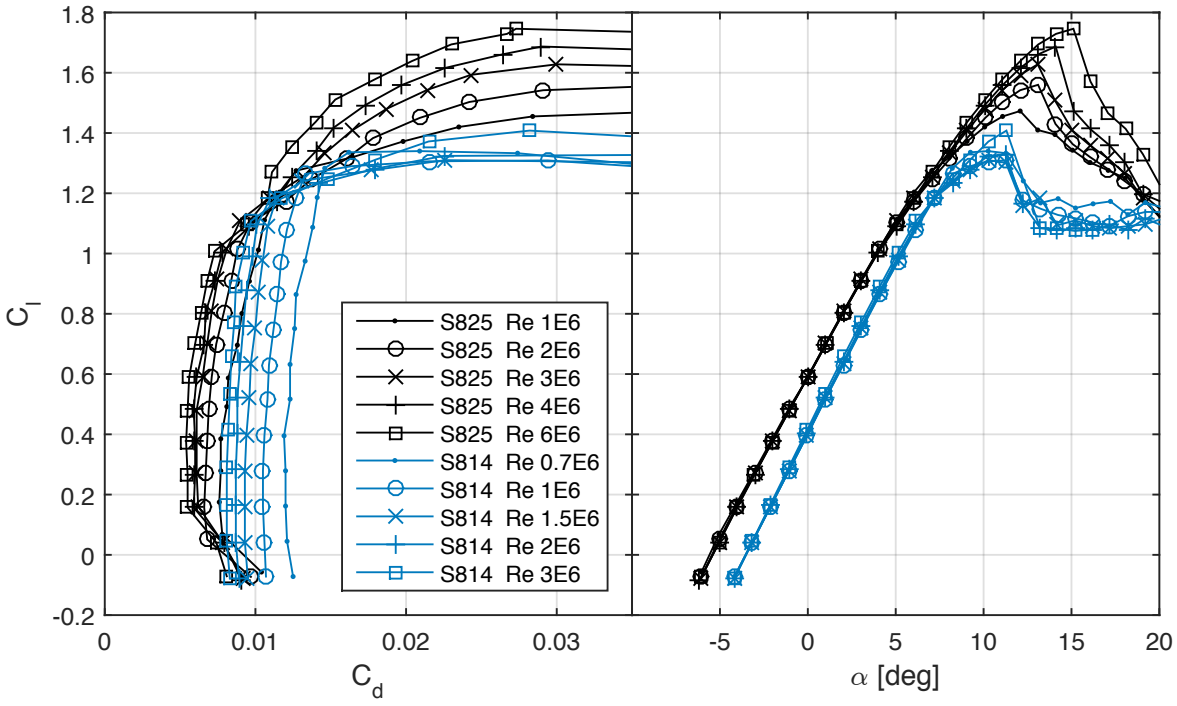

Figure 5.3. Experimental airfoil polars.

Table 5.1. AIRFOILS FOR SUBSCALE CIRCULATION MATCHING BLADE.

Section	Shape	$\frac{t}{c}$	$\frac{r}{R}$
1	Circle	1.0	0
2	S814	0.24	0.23
3	S825	0.17	0.49

The thicker (24%) S814 airfoil will be placed at a radial percentage of 0.23. This allows for adequate transition from a circle at the blade root to an airfoil shape. By mid-span and outboard, the blade has an S825 section, which is thinner (17%), and a higher lift-to-drag ratio. In board of $r/R = 0.23$, the airfoil transitions in shape to a circle. Since XFoil is not accurate for bluff bodies, a lift-to-drag ratio preserving interpolation was used as seen in Figure 5.4. A summary of the airfoils and their location are summarized in Table 5.1.

A few other user inputs have been implemented into the inverse design tool for practical reasons. The first is that the user must specify the maximum allowable twist and chord. Both of these keep the blade reasonable in shape to be manufactured for arbitrary lift and circulation objective functions which may lead to exceedingly large chord or twist especially inboard. To keep the array spacing equal to the designed SWiFT 3D, 5D, 6D, the blade radius is equal to $R = 13.5$ m, the maximum allowable twist is $\beta_{max} = 12°$, the maximum

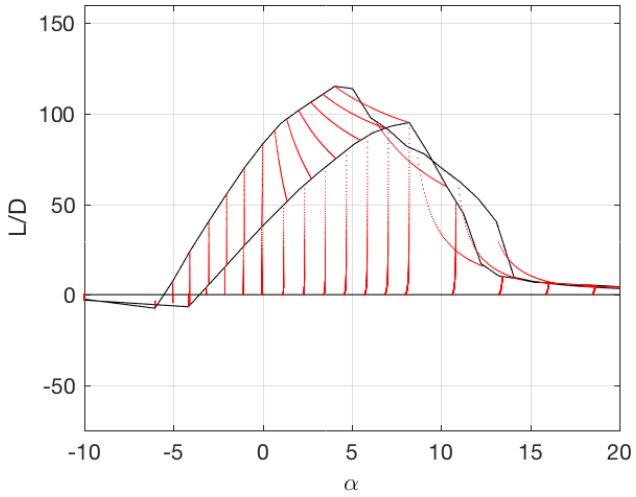

Figure 5.4. Lift-to-drag ratio characteristics of circle, S814, S825 airfoils.

chord is $c_{max}/R = 0.10$, the root chord is $c_{hub} = 0.5926$ m, and it mounts to the hub at a normalized radial distance $r_{hub}/R = 0.0370$. The blade geometry found with these constraints according to the scaled wake approach is presented in Chapter 7.

5.1 Inverse Design Algorithm

The process by which the blade is designed from the aforementioned constraints, is a follows. First the blade blade geometry initiated from $a = 1/3$ solution. Next WT_Perf is run to find the dimensionless circulation and lift coefficient across the blade. The difference between the current iteration and the target distributions, the residuals r_Γ, r_α, are found. The chord for the next iteration is determined by the error at every span station circulation residual. And the twist for the next iteration is determined by the current angle of attack residual, and its corresponding C_l. In equations, that is

$$c/R_{i+1} = c/R_i - k_1 r_\Gamma \tag{5.2}$$

and

$$\beta_{i+1} = \beta_i + k_2 r_\alpha. \tag{5.3}$$

The k_1 and k_2 constants were adjusted so that the solution converged. Two values that worked well were $k_1 = 0.33$ and $k_2 = 1.05$ for the aforementioned objective functions, and at least 50 iterations were required for adequate convergence.

5.2 Unsteady Dynamic Similarity

The time rate of change of circulation, $d\Gamma'/dt^*$, is responsible for spanwise vorticity being shed into the wind turbine wake. For similarity in gust response between the two blade scales the following relationship was developed showing that the time rate of change of dimensionless circulation should be constant for any size wind turbine to create a scaled wake due to spanwise shed vorticity.

$$C_{l_\alpha}\frac{c}{R}\frac{W}{U_\infty}\frac{d\alpha}{dt^*}+C_l\frac{c}{R}\frac{d(W/U_\infty)}{dt^*}=K. \tag{5.4}$$

For a given blade section, the angle of attack is determined by the relative velocity components. To be precise when scaling, the rate of change of angle of attack would have contributions from blade bending and twisting, yaw error, and changes in inflow velocity. The time rate of change of relative inflow velocity would have contributions from blade bending, yaw error, and turbulent inflow. To simplify, the first term is relatively large compared to the second term because the time rate of change of angle of attack is fast for small velocity and blade motions, whereas the second term is slow because the time rate of change of inflow velocity is dominated by the rotor angular velocity. Assume that out-of-plane bending is causing changes in angle of attack, such that the blade deflects harmonically $h = h_0\, e^{-i\omega_h t}$ and for small angles of attack $\alpha = \frac{\dot{h}}{\lambda r/R}$. The simplified scaled wake equation using only blade motion causing changes in angle of attack yields

$$C_{l_\alpha}\frac{c}{R}\frac{h_0}{R}\left(\frac{\omega_h}{\Omega}\right)^2\lambda^2=K. \tag{5.5}$$

Therefore the gust response factor should be held constant between scales so that the shed spanwise vorticity in time occurs at the same rate and amplitude across the entire blade span. The product of the blade tip deflection and the ratio of blade bending frequency to rotor frequency squared appear. This is where the structural design should be considered in conjunction with the aerodynamic design of a blade the exactly recreates a scaled wake. It remains an open question how important this term is to the evolution of the wake.

5.3 Similarity Summary

To summarize, similarity has been given up in a few areas, with the intention to design a subscale wind turbine that produces a wake with similitude to a full-scale wind turbine. The NRT is not a geometrically scaled GE 1.5sle turbine. Kinematic similarity is maintained with equal tip-speed-ratios and with nearly equal ranges of atmospheric inflow conditions. Dynamic similarity is partially maintained by keeping the ratio of lift forces equal across the span of the blade which is the most important force for creating a wake. The effect of drag on axial and tangential loading has been ignored.

- Kinematic similarity - λ, tip vortex spacing, helix angle, and wake structure in region 2
- Dynamic similarity - Γ', a, and C_T in region 2
- Not designed to scale - Re_c, Re_D, C_d, L/D, C_P, $\frac{c}{R}$, β, C_l, airfoil shape, gust response, and aeroelasticity

With the known airfoil locations, the following constraints fully define the problem to solve for chord and twist along the blade span.

$$\Gamma'_{ss} = \Gamma'_{fs}, \quad \frac{r}{R} \in [0,1] \tag{5.6}$$

$$C_{lss} = 0.6, \quad \frac{r}{R} \in [0, 0.97] \tag{5.7}$$

$$c(1)_{ss} = \frac{c(1)_{fs} c(0.9)_{ss}}{c(0.9)_{fs}}. \tag{5.8}$$

Chapter 6

Blade Tip Design

Blade tips are a great source of noise. Dipole-type sources of noise radiate acoustic power proportional to the relative velocity to the sixth power. The greatest relative velocity on a blade is at the tip and almost equal to the tip speed at high tip-speed-ratios. The speed of the new NRT blade is 62 m/s, lower than the full-scale blade that would have a tip speed around 70–85 m/s. Because this new blade design has a different tip speed than the full-scale blade it will not be suited for scaled acoustics tests operating the turbine at its current maximum speed of 43.9 rpm. The new rotor would need to spin at over 50 rpm to match the tip speed of a full-scale rotor.

Circulation and lift coefficient targets determined a unique chord and twist over the entire blade. However, this led the a relatively large finite chord at the tip. Therefore, the lift coefficient constraint was removed outboard of 97% span, and instead the chord was forced to taper such that the ratio of chords of full-scale and subscale were equal at 90% and 100% span, that is

$$c(100)_{ss} = \frac{c(100)_{fs}\, c(90)_{ss}}{c(90)_{fs}}. \tag{6.1}$$

In addition, the subscale chord curvature was chosen such that the transition at 97% span was smooth with the scaled, tapered tip. Twist was still adjusted to enforce the circulation matching over the entire span, even outboard of 97% span. This method led to the chord distribution seen in Figure 6.1. Notice the chords at 90% and 100% span normalized by the blade 90% span chord are equal.

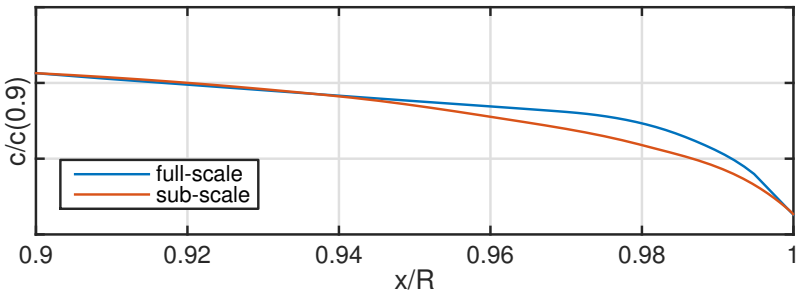

Figure 6.1. Scaled tip design.

Chapter 7

Inverse Blade Design Results

The inverse design tool has been implemented in MATLAB. Once the user has specified the target circulation distribution, target lift coefficient, tip-speed-ratio, air density, airfoil aerodynamic data, shape, and locations, the inverse design tool converges on the objective functions. The sum of the root mean square errors are seen to tend towards zero, showing the design is converged as seen in Figure 7.1. The minor increase in error seen at the converged solution occurs due to the scaled tip design being added.

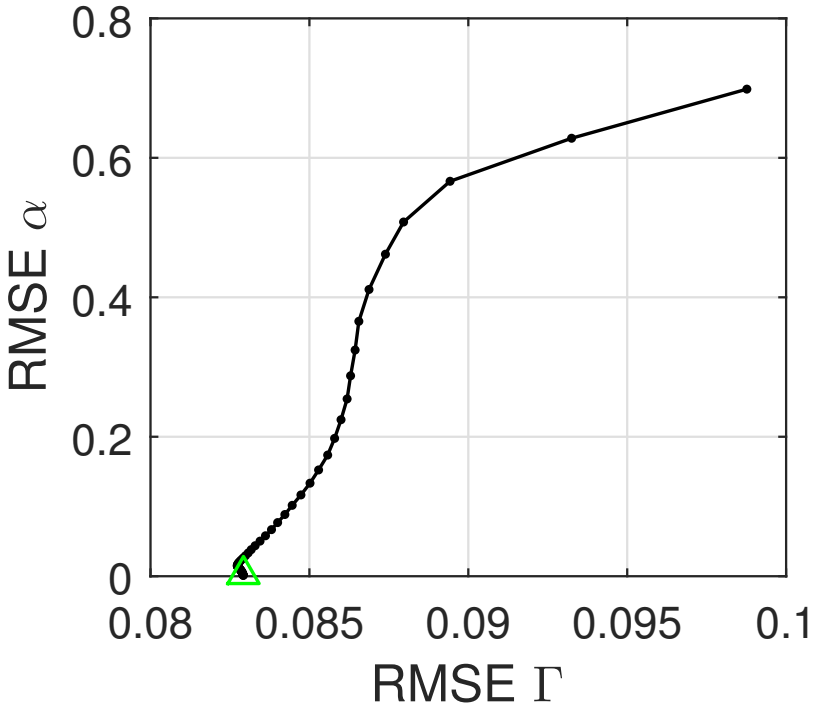

Figure 7.1. Root mean square error at every iteration showing convergence of geometry on objective circulation and angle of attack.

The full-scale circulation, Γ'_{fs} , is the main objective function that the solution converges towards to recreate the wake of a full-scale wind turbine. It should be noted that this

objective function was found through analysis with WT_Perf for a commercial wind turbine that is rated at 1.5 MW. The airfoils used were from clean surface wind tunnel data. The WT_Perf input file was created based on data provided by the manufacturer, and the full-scale rotor was simulated at a tip-speed-ratio of 9, slightly higher than in real operation. But, this high tip-speed-ratio was chosen to be representative of a modern, highly efficient wind turbine. In general, the objective circulation, Γ'_{fs}, can be specified by the user for any spanwise distribution desired.

The dimensionless circulation results of the subscale blade are plotted with the objective function seen in Figure 7.2. The control points lay nearly on top of the objective function. The shape of the intermediate points in the root region from $0.05 < r/R < 0.2$ cannot be precisely controlled as its shape is determined by the aerodynamic interpolating near stall. However there is already uncertainty in root aerodynamics due to 3D flow and the prediction of bluff body aerodynamics. The magnitude of the ordinate has been removed due to the proprietary nature of the full-scale blade design. This plot clearly shows that the circulation matching requirement has been met.

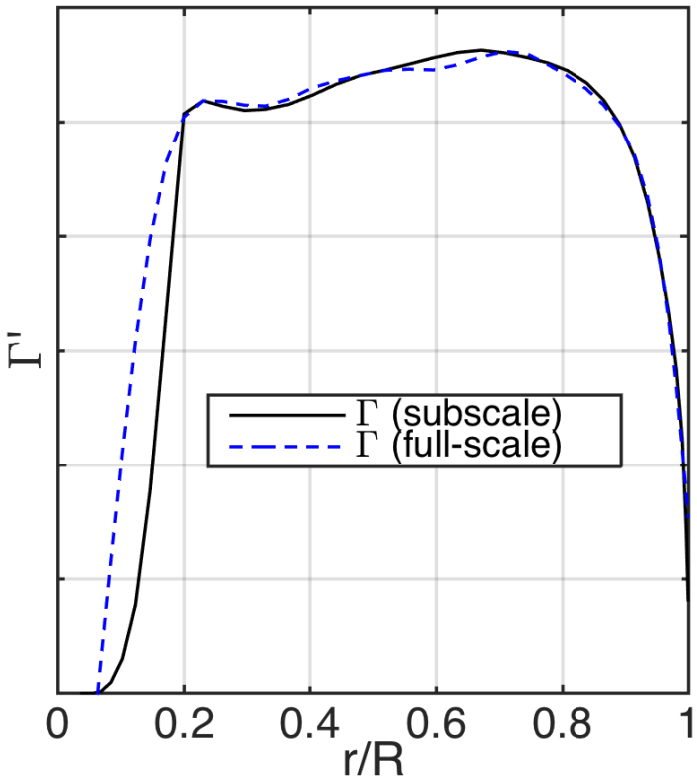

Figure 7.2. Circulation along blade span matching objective function (full-scale).

The lift coefficient for the subscale blade is plotted in Figure 7.3. The lift coefficient is clearly not at maximum efficiency. But in region 2 there needs to be a margin of error so that the blade can reach rated power in region 3 without stalling since this is a variable speed, variable pitch design. The outer half of the blade matches the intended constant lift coefficient distribution, $C_l = 0.6$.

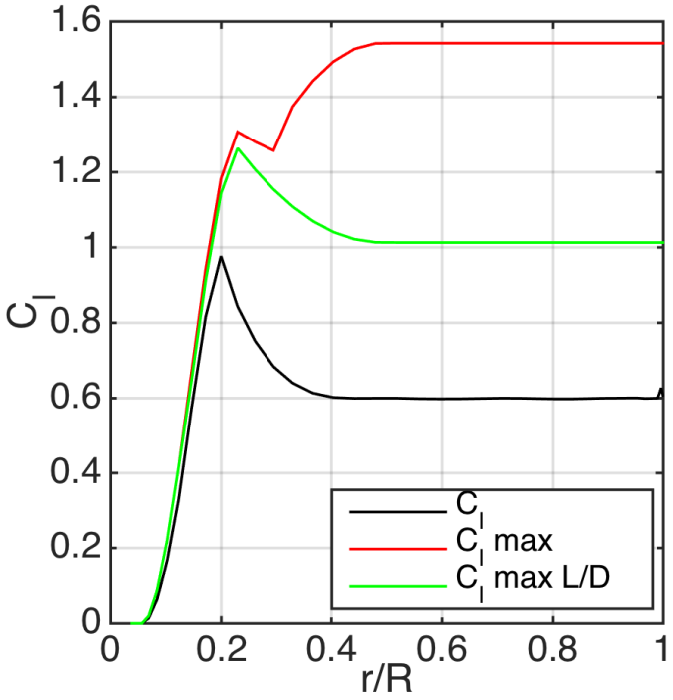

Figure 7.3. Lift coefficient along blade span with a stall margin and higher solidity for interior instrumentation.

Based on the specified airfoils of a circle, S814, and S825, Figure 7.5 shows the final shape as viewed from the blade tip. It should be noted that Wetzel Engineering added prebend not reflected in this image. The maximum chord has been limited to 11% of the span, and the maximum twist has been limited to 12.1°. This is the cause of not achieving linear lift coefficient variation across the inboard region.

The chord and twist distribution are plotted in Figure 7.6. The solidity of the rotor is $\sigma = 6.4\%$. The subscale design is shown with a maximum efficiency rotor dimensions (lower solidity), and the Vestas V27, the blade being replaced by the current design. This provides a visual check that the new design is not drastically different than the OEM blade.

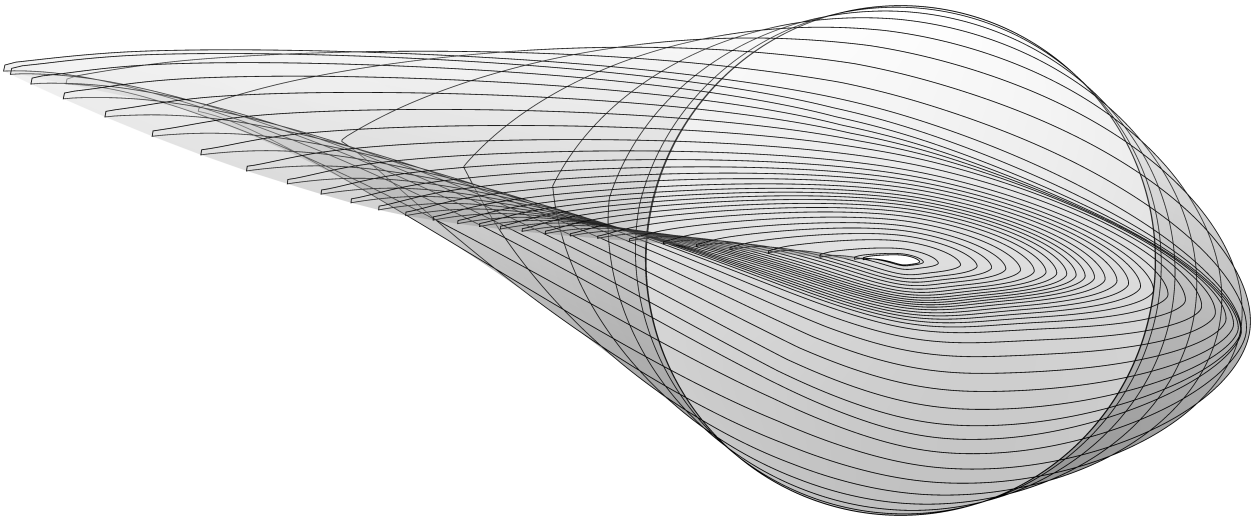

Figure 7.4. End view from tip of blade sections.

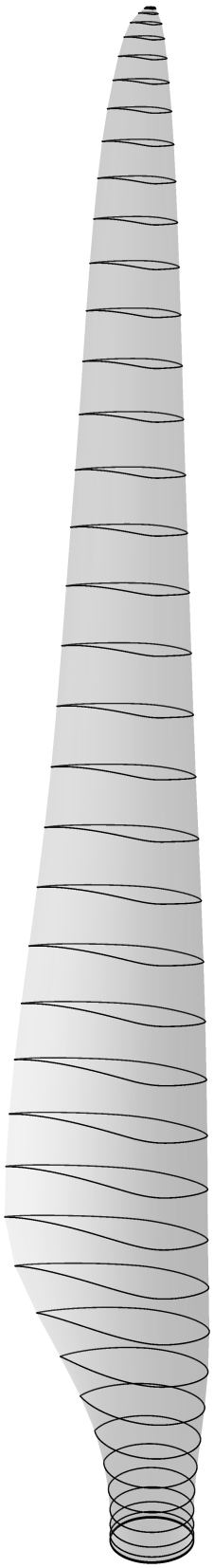

Figure 7.5. Isometric view of NRT blade and sections.

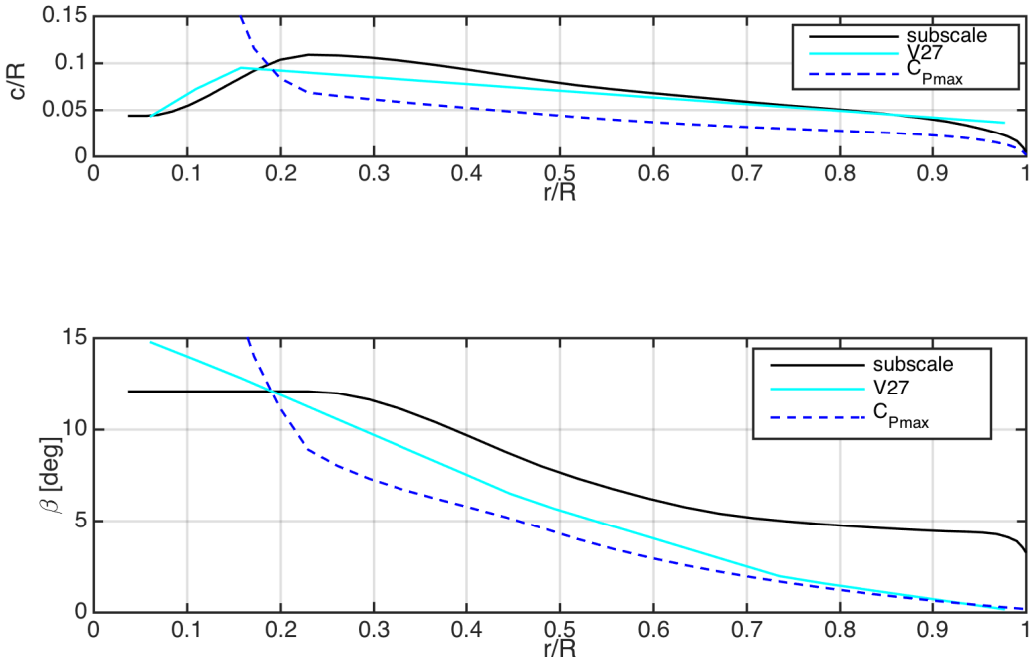

Figure 7.6. Chord and twist distributions for new NRT blade.

Chapter 8

Blade Performance

The blade rotor diameter was chosen to be $D = 27$ m to keep the array spacing equal to the designed 3D-5D-6D at SWiFT. The turbine will be operated as a variable speed, variable pitch machine. In region 2, the tip-speed-ratio was chosen to be 9, similar to modern full-scale turbines that are high efficiency. The operating parameters include a rated power of 195 kW, a cut-in wind speed of 4 m/s, a cut-out wind speed of 15 m/s, the maximum rotor speed of 48.70 rpm, a gearbox ratio of 27.6, and the average air density at SWiFT is 1.08 kg/m^3. The power curve and performance of the blade were modeled in WT_Perf [8] and the power curve is plotted in Figure 8.1. The power coefficient in region 2 is $C_P = 0.461$, and the thrust coefficient is $C_T = 0.861$. A wind speed of 7.65 m/s divides regions 2 and 2.5, and a wind speed of 11.11 m/s divides regions 2.5 and 3. The high-speed-shaft torque constant required to achieve region 2 of operation is 2.506×10^{-4} Nm/rpm^2, and in region 2.5 and 3, the maximum high-speed-shaft torque is 1385 Nm. The necessary blade pitch to keep the power fixed at 195 kW beyond a wind speed of 11.11 m/s is shown in Figure 8.1. The performance of the blade at various wind speeds is plotted in Figure 8.3.

To predict the annual energy production, meteorological data was analyzed for the SWiFT site. A wind site analysis was used to find the probability density function that described the probability of wind speeds at hub height.

$$Pr(U_\infty) = \frac{k}{l}\left(\frac{U_\infty}{l}\right)^{k-1} e^{-(U_\infty/l)^k}. \tag{8.1}$$

At SWiFT the shape factor is $k = 2.773$, and the scale parameter is $l = 7.499$. Figure 8.2 shows the area, or probability, associated with how often the winds at hub height are in region 2, 2.5, or 3. These results are summarized in Table 8.1. The capacity factor or percent of time operating at rated power, cf, is 30.0%. The probability at any moment the wind turbine will be operating in region 2 is 49.2%. The probability that the wind turbine is at maximum speed but below rated power (region 2.5) is 29.7%. The 3 blades have a planform area that is 6.4% of the swept area, also known as solidity, σ.

Table 8.1. SUMMARY OF BLADE PERFORMANCE.

D [m]	λ_{R2}	σ [%]	P_{rated} [kW]	$C_{P_{R2}}$	$C_{T_{R2}}$	Pr(R2)	Pr(R2.5)	Pr(R3)	cf	AEP [GWh]
27	9	6.4	195	0.461	0.861	0.492	0.297	0.0500	0.300	0.512

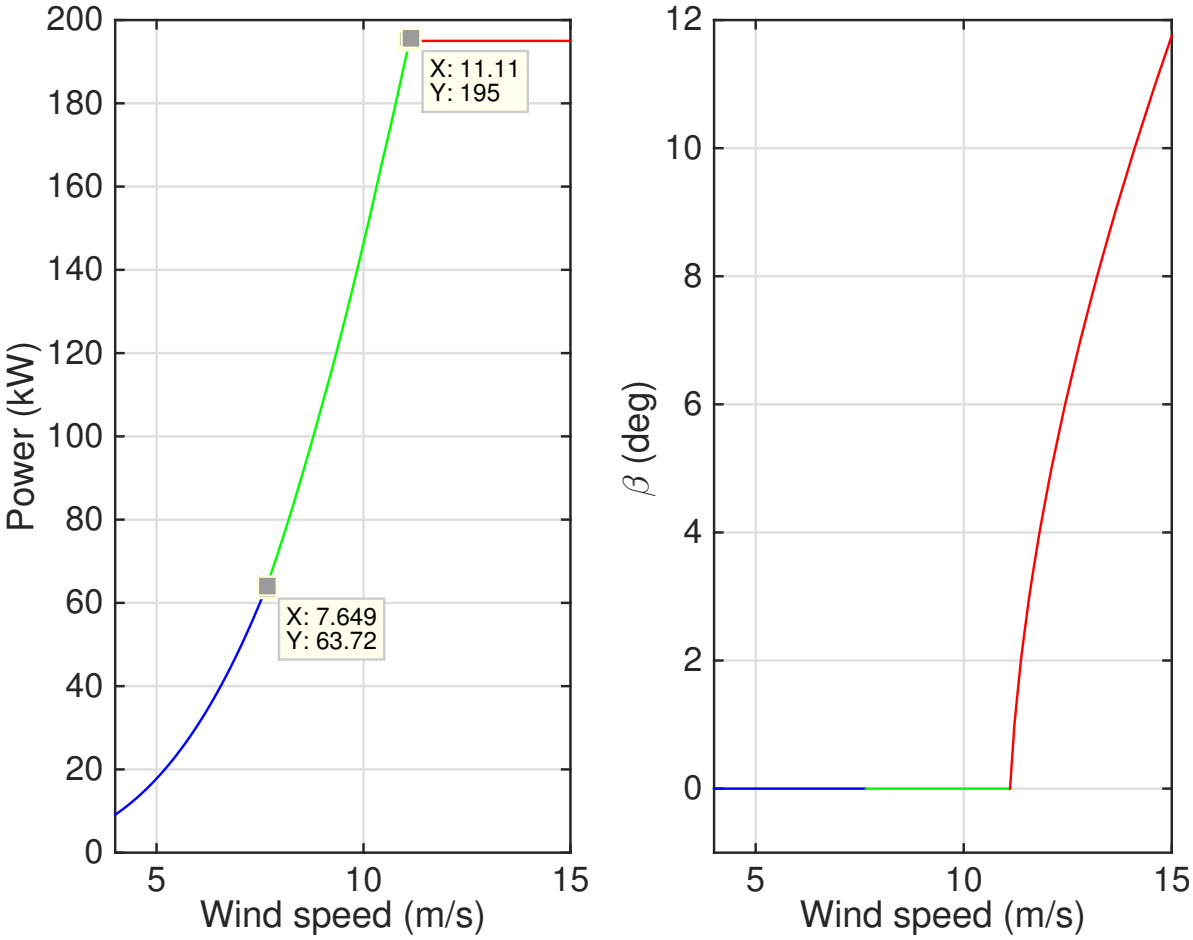

Figure 8.1. Power curve for NRT rotor design and pitch schedule.

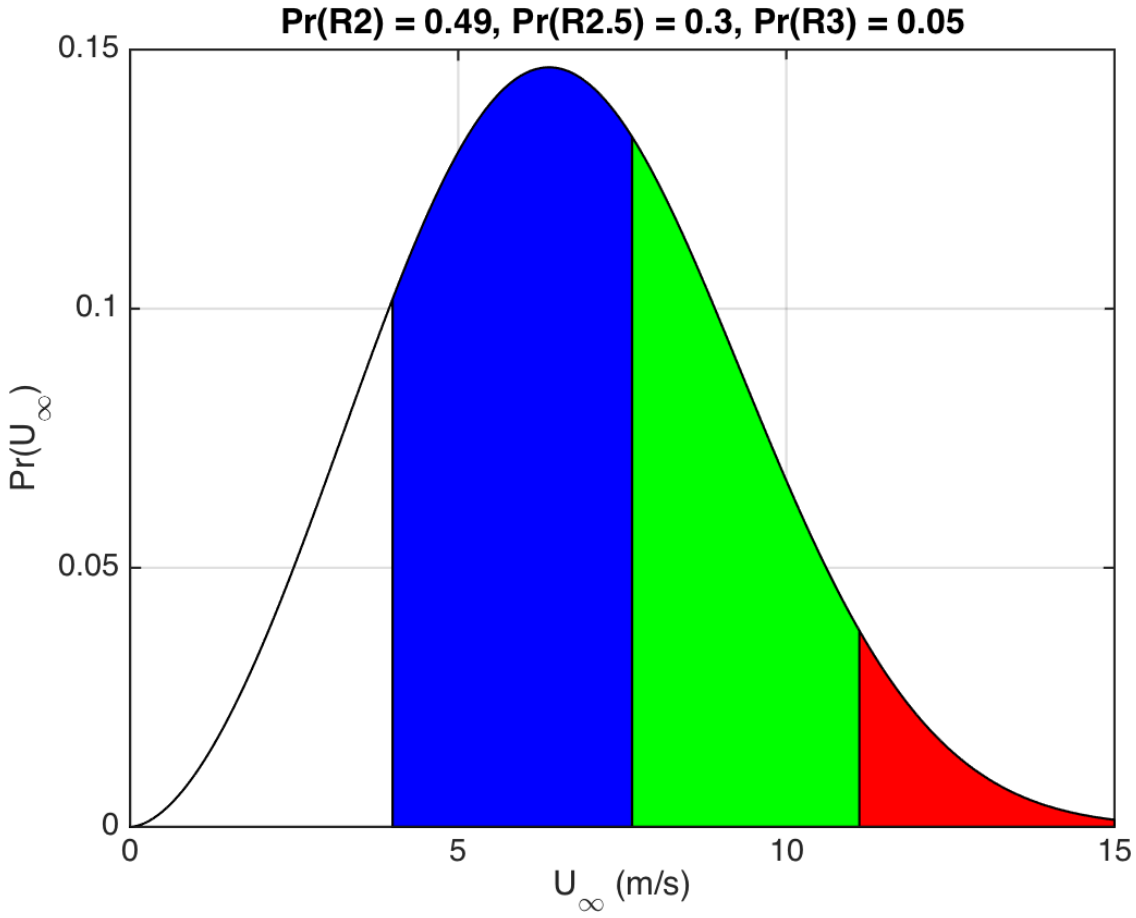

Figure 8.2. Probability of regions of operation.

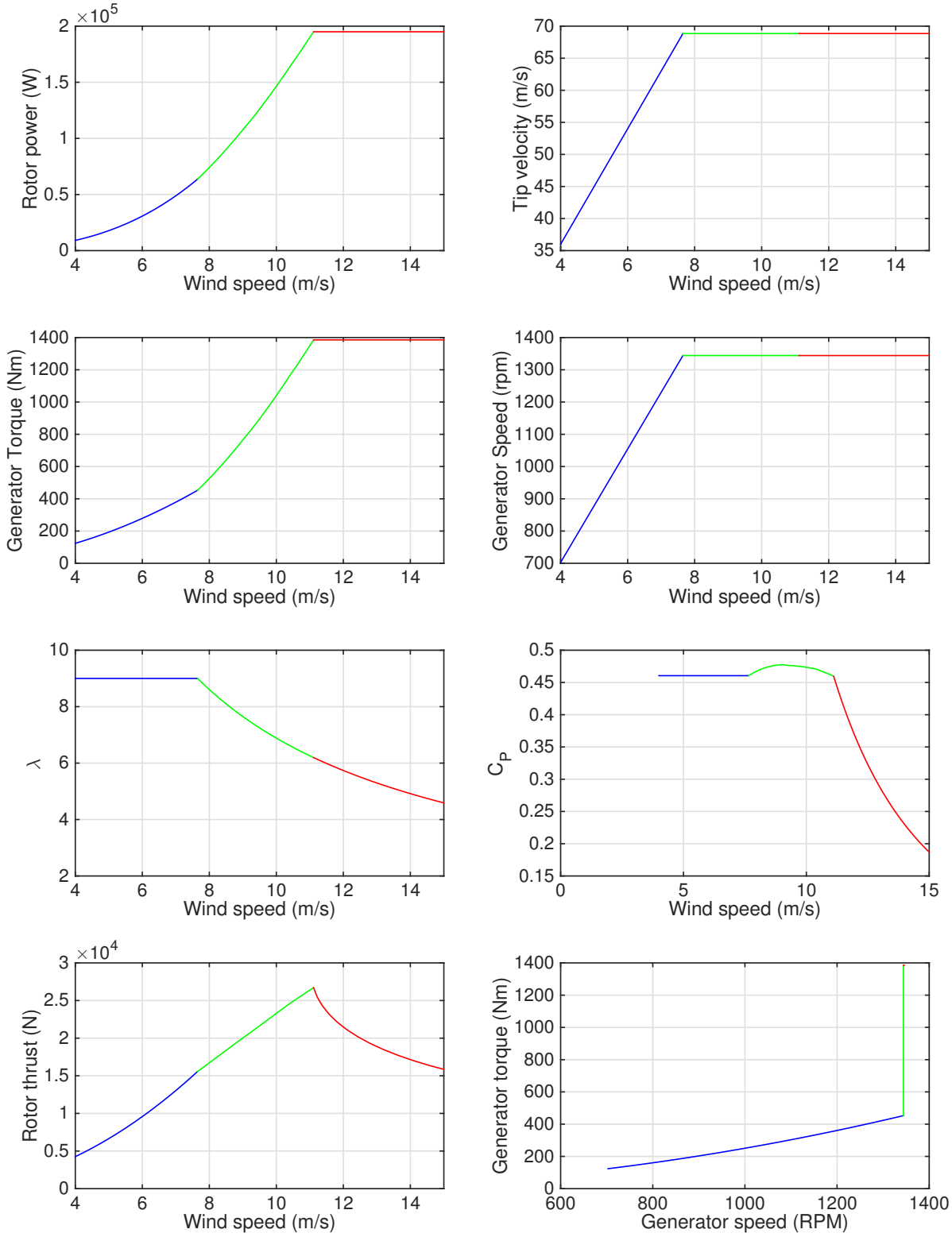

Figure 8.3. Performance curves.

Chapter 9

Performance at Span Stations

This chapter shows how different aerodynamic quantities vary across the blade span for five different wind speeds, 6.6 m/s, 9 m/s, 11 m/s, 13 m/s, and 15 m/s. These wind speeds correspond to the median wind speed at SWiFT, two wind speeds in region 2.5 of operation, and two wind speeds in region 3 where the blade begins to feather to regulate power. The new blade spends 38% of the time in region 2.5 of operation where tip-speed-ratio is not constant and below the optimal value of 9. This causes the angle of attack to increase in region 2.5. In region 2, the inner 16% of the blade span is stalled, and by the top of region 2.5, the inner 36% of the blade is stalled as seen in Figure 9.1. Continuing into region 3, because the blade starts to pitch towards feather, the angle of attack is reduced over the entire blade span as wind speed increases. For completeness, Figures 9.2–9.10 show how lift, drag, lift-to-drag ratio, Reynolds number, torque per unit length, thrust per unit length, dimensionless circulation, and induction vary across the blade span at the same five wind speeds.

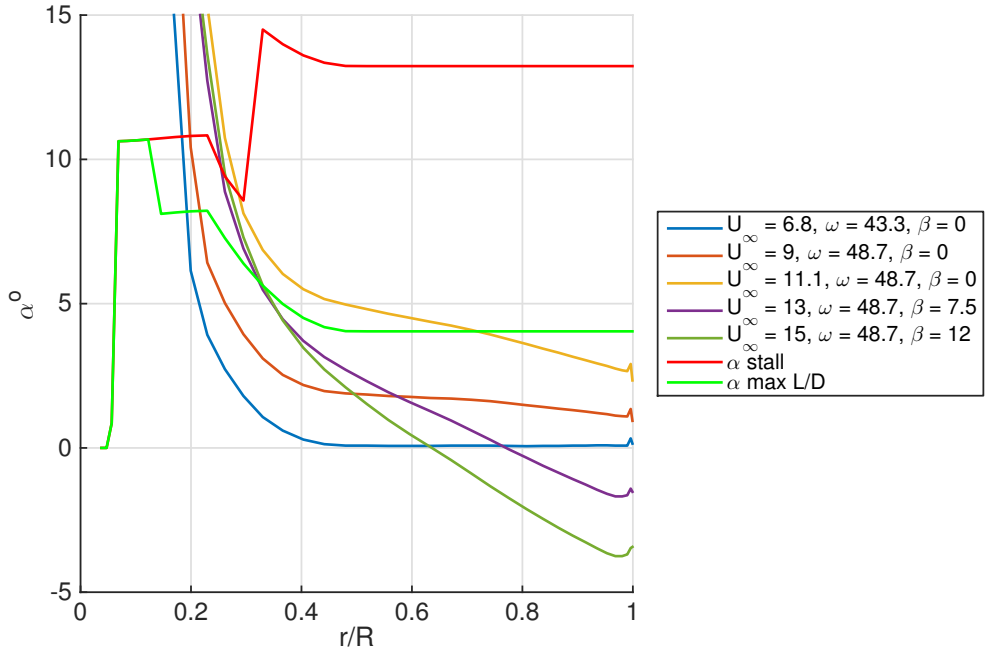

Figure 9.1. Angle of attack for NRT rotor design.

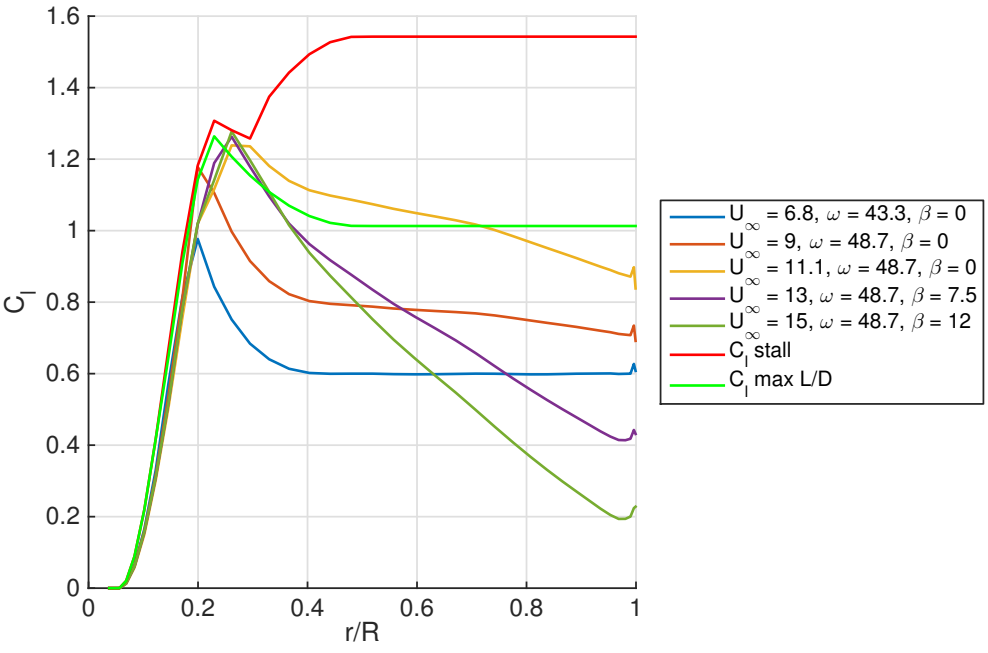

Figure 9.2. Lift coefficient for NRT rotor design.

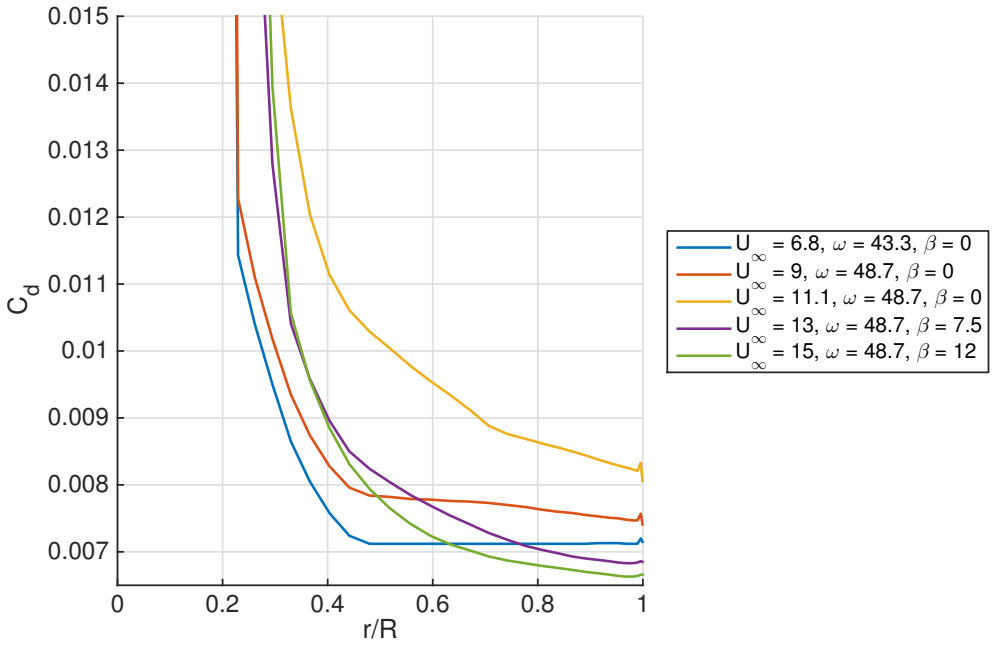

Figure 9.3. Drag coefficient for NRT rotor design.

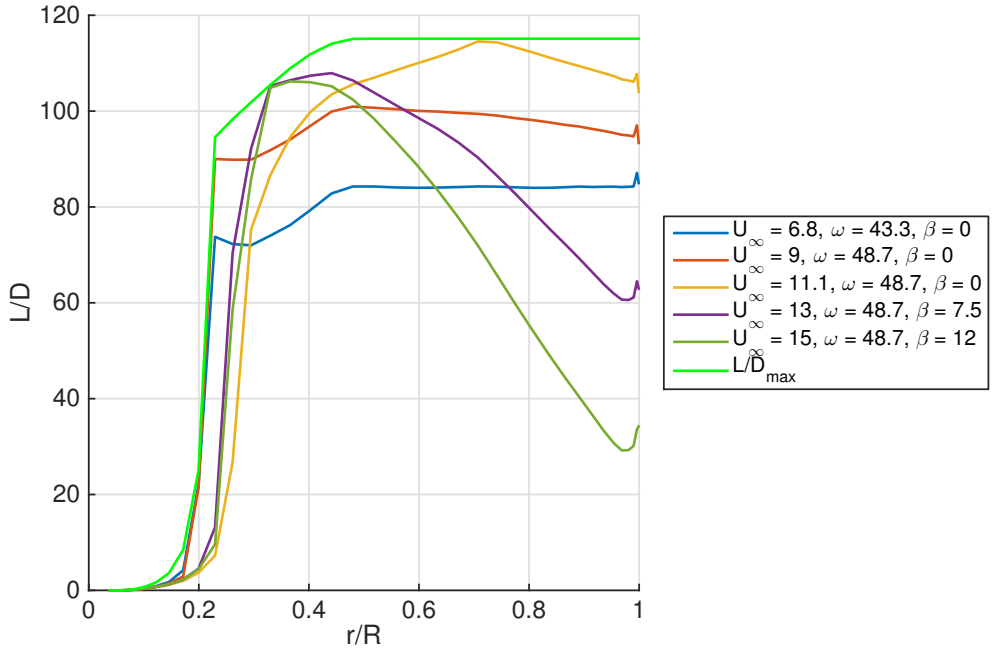

Figure 9.4. Lift-to-drag ratio for NRT rotor design.

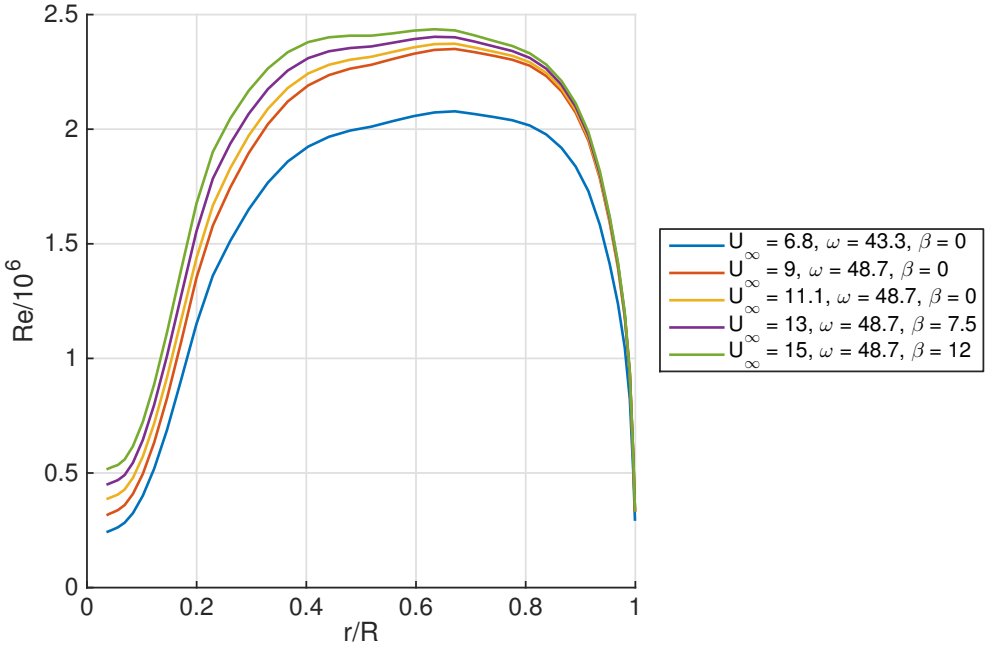

Figure 9.5. Reynolds number for NRT rotor design.

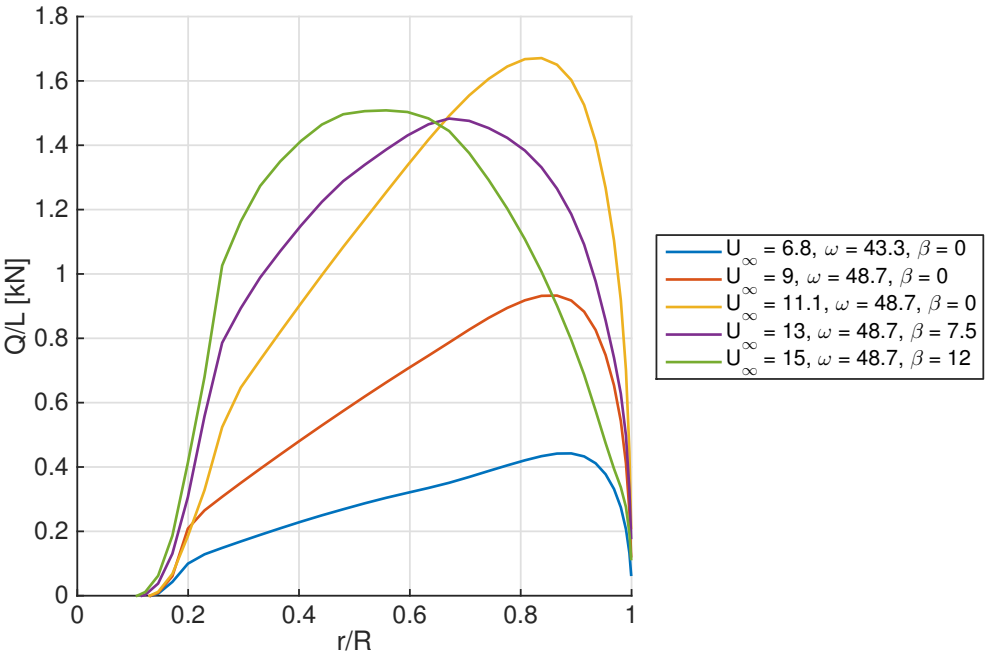

Figure 9.6. Torque per unit length (per blade) for NRT rotor design.

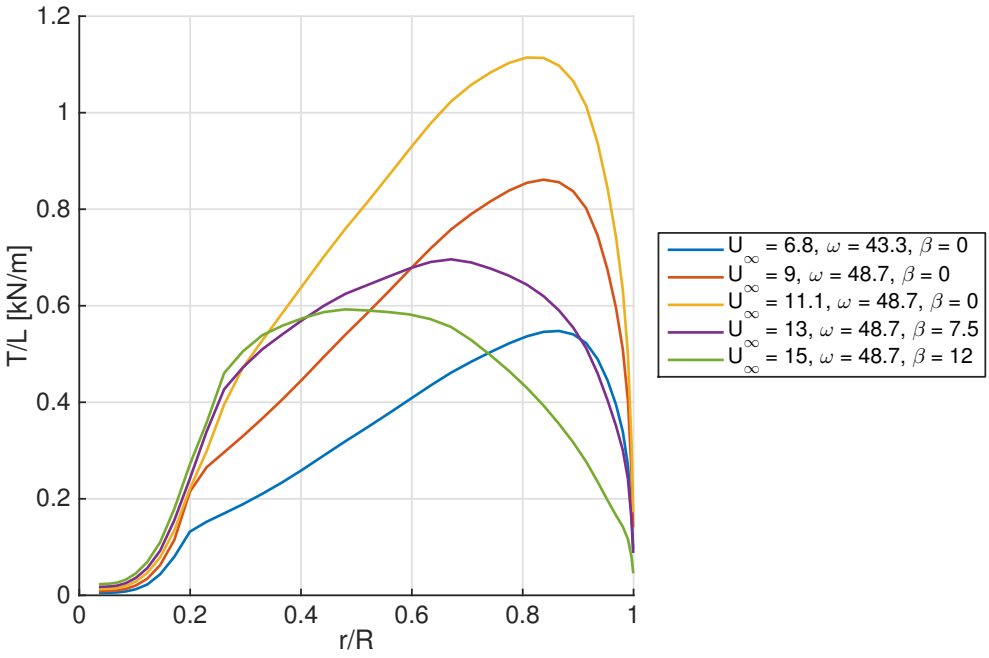

Figure 9.7. Thrust per unit length (per blade) for NRT rotor design.

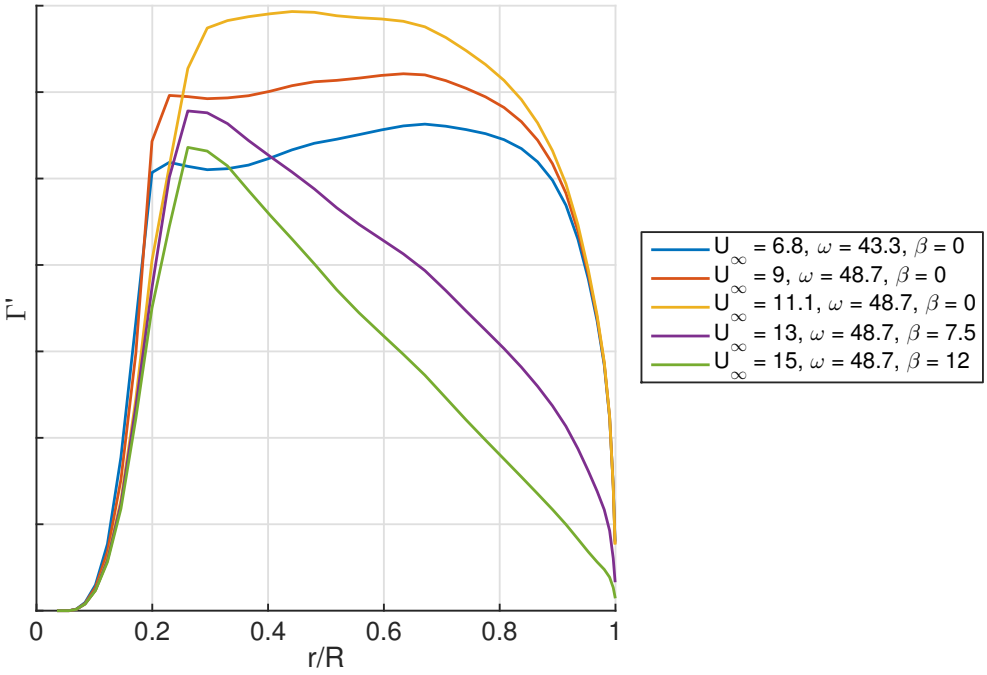

Figure 9.8. Dimensionless circulation for NRT rotor design.

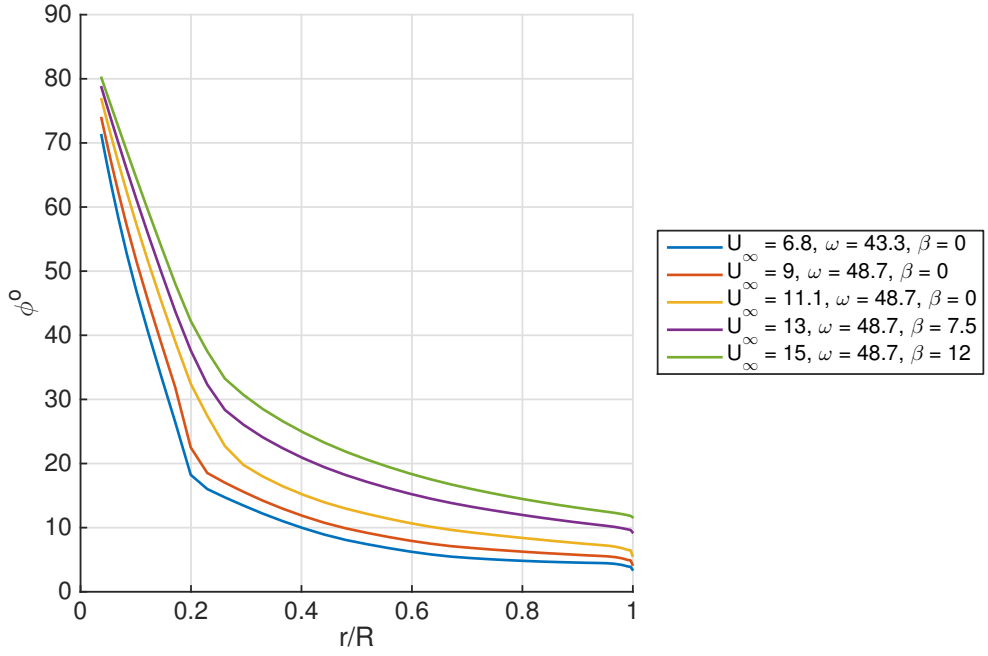

Figure 9.9. Inflow Angle for NRT rotor design.

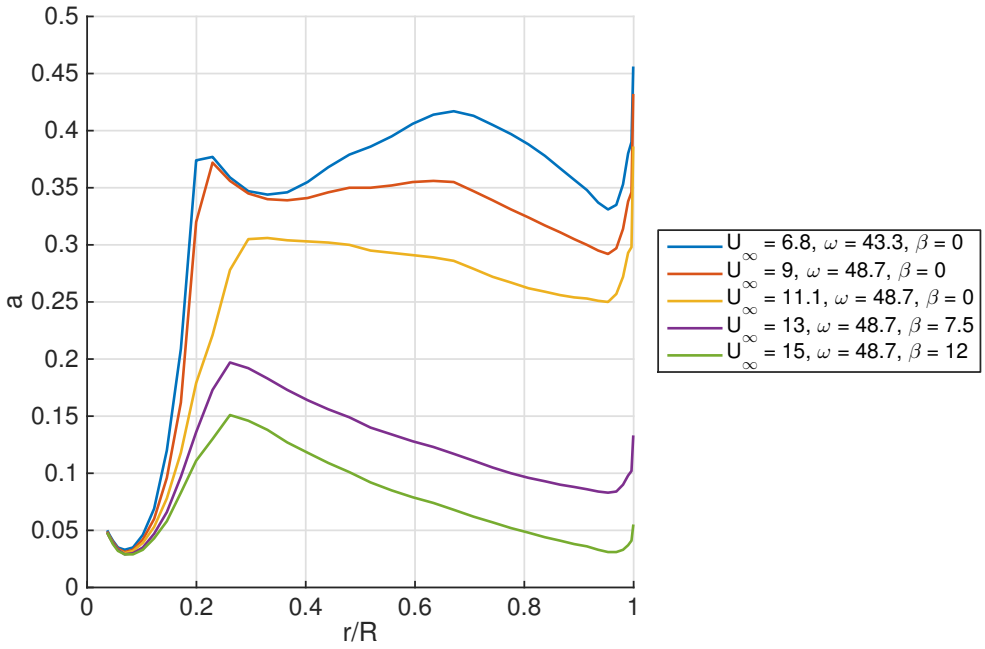

Figure 9.10. Induction for NRT rotor design.

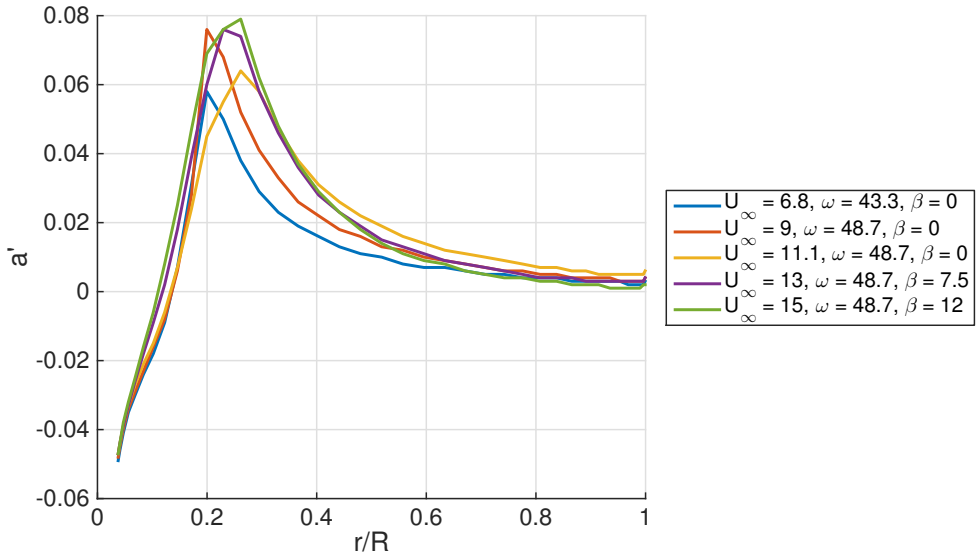

Figure 9.11. Tangential induction for NRT rotor design.

Chapter 10

Blade Sweep

For safe operation of the new subscale wind turbine, it is desired that in the event of hydraulic pressure loss for the blade pitch system, the aerodynamic moments will twist the blade to feather (airfoil nose down). At all wind speeds, it is desired that the new subscale blade have the same or more negative root twisting moment as the V27 turbine. Sweep was handled after the aerodynamic design, and so it is assumed there is no aeroelastic coupling.

To meet this requirement, three different sweep design were compared to the V27 root twisting moment. The sweep designs included a straight leading edge, an aerodynamic center aligned with pitch axis, and maximum section thickness aligned with the pitch axis. The first design had the largest nose-down pitching moment but was excessively large in magnitude and would slow down the blade pitch rotation towards run. With the aerodynamic center at pitch axis lift does not contribute to blade torsion, but again the nose-down moment was too large because the S-series airfoils have large camber moment coefficients 3 times larger than the V27 NACA airfoils.

The sweep design chosen placed the maximum thickness location at the pitch axis. Figure 10.1 compares the relative contributions of moment coefficient and normal force coefficient causing torsion per length along the blade. The blade uses positive cambered airfoils, so the moment coefficient contributes significantly to static stability ($C_m \approx -0.16$), but is partially canceled out by the normal force coefficient on the outer half of the blade. The total torsion per length T/L [kN] is shown in the right part of Figure 10.1. The maximum chord region contributes the most towards feather stability because the lift and moment produce a torque towards feather. Despite the distribution of moments and forces being different between the two designs, the magnitude of the root torsion on the subscale design is greater or equal to the OEM blade.

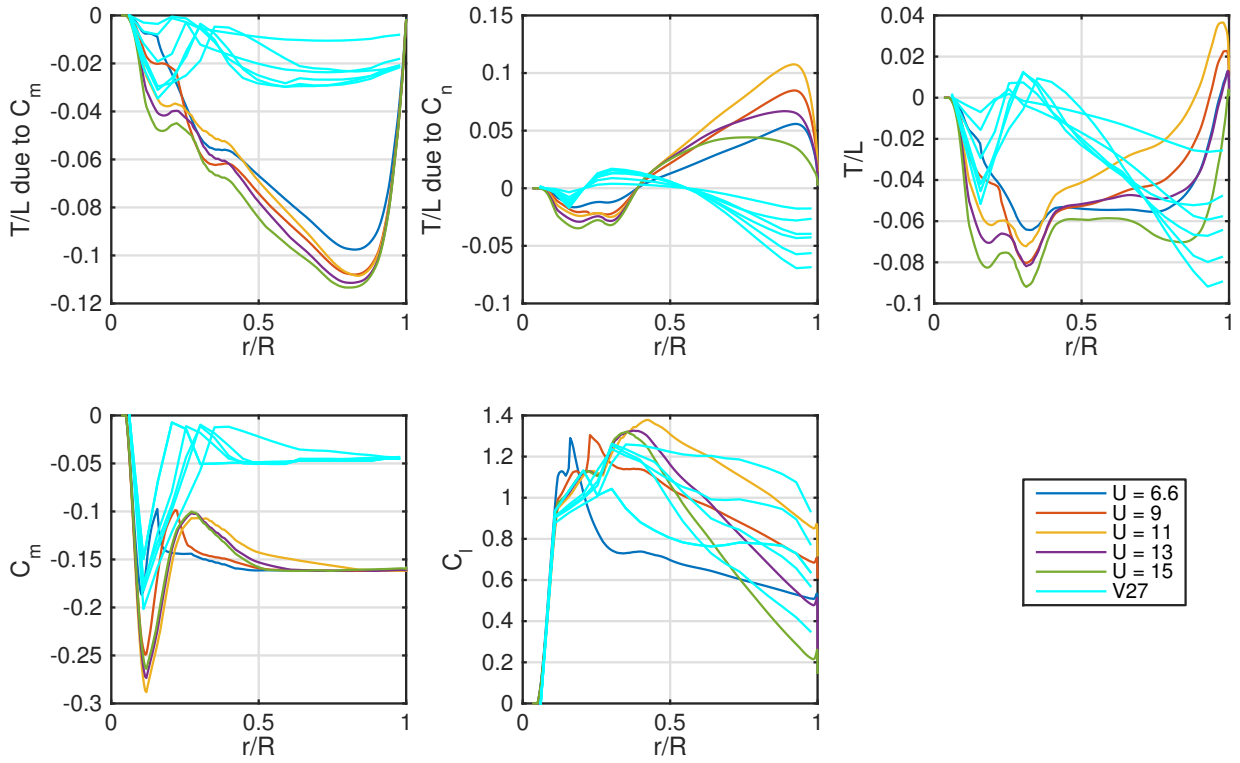

Figure 10.1. Torsion per unit length due to moment coefficient and normal force coefficient.

Chapter 11

Requirements Overview

Building and flying a new blade design is a big investment. A number of important flow physics and turbine-turbine interaction experiments are planned to test these new blades. Planning an experiment for an existing turbine and nacelle with new blades means there are a number of requirements to safely operate the turbine, and to allow for flexibility of many potential experiments planned. How these requirements flow down from a project planning perspective, the reader is referred to the National Rotor Testbed Requirements [9]. This chapter summarizes what the aerodynamic design requirements are and how they have been met.

11.1 Variable Speed, Constant Tip-speed-ratio

The existing wind turbine at SWiFT has a variable speed generator that will remain the same for the new NRT blades. This means that the rotor rotational velocity increases proportionally with wind speed. This also allows for a range of wind speeds of constant tip-speed-ratio operation before the maximum rotational speed of the generator is reached. A tip-speed-ratio of $\lambda = 9$ is relevant to full-scale turbines in region 2, and by the previous kinematic similarity argument, should be maintained for the subscale design. Figure 8.1 shows this requirement is met from cut-in, 4 m/s, to 6.9 m/s and will operate here 39% of the time based on meteorological analysis at SWiFT.

11.2 Equal Dimensionless Circulation Distribution Across Span

From steady analysis, the shed vorticity and creation of the wake is determined by the circulation distribution across the blade span. Therefore the new subscale design's circulation must match the full-scale circulation, $\Gamma'_{fs} = \Gamma'_{ss}$. This requirement was met by the inverse blade design process, and is plotted in Figure 7.2. And the sum of the root mean square error at 199 blade stations is below 0.085 for Γ'.

11.3 Equal Power Coefficients

Full-scale wind turbines use high lift-to-drag ratio airfoils at high Reynolds numbers and high tip-speed-ratios to achieve excellent efficiency. By scaling down the new design, new airfoils were chosen. The S825 still achieves L/D in excess of 100 at a Reynolds of 1.5×10^6. The new blade as designed has a higher solidity than optimal to maximize power coefficient, as seen in Figure 7.6. Nonetheless, the subscale design was analyzed in WT_Perf and achieved a power coefficient of 0.47, 2.1% below the full-scale rotor, $C_P = 0.48$ This meets the 5% requirement, $C_{P_{ss}} = C_{P_{fs}}(1 \pm 0.05)$.

11.4 Equal Dynamic Loading (Gust Response)

The time rate of change of circulation, $d\Gamma'/dt^*$, is responsible for spanwise vorticity being shed into the wind turbine wake. This value should be held constant for all cases of a scaled rotor due to blade elasticity, yaw error, and wind shear.

$$C_{l_\alpha} \frac{c}{R} \frac{W}{U_\infty} \frac{d\alpha}{dt^*} + C_l \frac{c}{R} \frac{d(W/U_\infty)}{dt^*} = K. \tag{11.1}$$

Due to the complexity of terms and the interaction of structural design with aerodynamic design, (even for the simple cases of only considering blade elasticity without yaw error and shear) this requirement has not been met. The simplified scaled wake equation using only blade motion causing changes in angle of attack yields

$$C_{l_\alpha} \frac{c}{R} \frac{h_0}{R} \left(\frac{\omega_h}{\Omega} \right)^2 \lambda^2 = K. \tag{11.2}$$

Also it is already known that the subscale solidity, c/R is higher than full-scale, 6.1% versus 4.7%. Therefore the gust response factor is different by the product of the blade tip deflection and the ratio of blade bending frequency to rotor frequency squared. It remains an open question how important this term is to the evolution of the wake.

11.5 Scaled Tip Design

Aeroacoustics and tip design are not a current driver for design. Therefore, Chapter 6 showed the tip design is a scaled version of the full-scale turbine. Outboard of 97%, the lift coefficient constraint was not enforced. This allowed for the chord to smoothly transition to the $c_{ss}(100)$ value based on geometric scaling discussed in Chapter 6.

11.6 Design for Analysis

Only two airfoils have been used in the blade design. This keeps the importance of airfoil polar interpolation to a minimum. The geometry should be sufficiently simple to mesh for CFD. The coordinates have already been exported as a point cloud of coordinates and meshed for CFD analysis in OVERFLOW with minimal effort. The effect of roughness introduces uncertainty in modeling. However the aerodynamic data for both S-series airfoils includes fixed transition and/or roughness tests from experiments at the Delft University of Technology Low Turbulence Tunnel (LSL) and the NASA Langley Low-Turbulence Pressure Tunnel [6, 7]. Therefore, future modeling efforts to predict the performance with soiling is possible.

11.7 Addressing Issues of Scale in Atmospheric Boundary Layer

Chapter 4, showed that on an average day, the shear for the subscale and full-scale turbines can be equal for unstable conditions from 11:00–17:00, and equal during the evening neutral boundary layer, 18:00–19:00 local time. Unfortunately, the average turbulence intensity at hub heights of the subscale is consistently lower than the full-scale by 2%. This does not make testing impossible at lower turbulence intensities, but will increase calendar time waiting for lower than average turbulence intensities.

Chapter 12

Conclusions

A new inverse wind turbine design tool has been implemented to design the outer shape of wind turbine blades that produce scaled wakes. This is accomplished by having similarity to full-scale wind turbines by having equal dimensionless circulation distributions for both scales. Geometric similarity was given up since Reynolds number cannot be held constant, but kinematic similarity was achieved by keeping tip-speed-ratios constant. The circulation objective did not fully define the problem, so the subscale lift coefficient distribution was also chosen to suit the needs of the subscale experimental campaign which lead to a solidity sufficient for internal instrumentation. The blade chord and twist were then found using the inverse design method. Analysis of the meteorological data at SWiFT revealed that equal dimensionless shear is observed on the average day between 11:00-19:00 local time, however the turbulence intensity at the subscale is consistently 2.5% higher than the full-scale turbine. Free-wake vortex simulations or large eddy simulations should be carried out to verify that circulation matching is the right approach to create wakes with similitude. Three-dimensional simulations using OVERFLOW are planned to deal with the uncertainty of the root to airfoil transition, and the effect of 3D, spanwise flow on blade performance.

References

[1] Christopher L Kelley, David C Maniaci, and Brian R Resor. Horizontal-axis wind turbine wake sensitivity to different blade load distributions.

[2] Xiaolei Yang, Aaron Boomsma, Fotis Sotiropoulos, Christopher L Kelley, David C Maniaci, and Brian R Resor. Effects of spanwise blade load distribution on wind turbine wake evolution. 53rd AIAA Aerospace Sciences Meeting, 2015.

[3] J. H. Strickland, B. T. Webster, and T. Nguyen. A vortex model of the darrieus turbine: An analytical and experimental study. *Journal of Fluids Engineering*, 101(4):500, 1979.

[4] J. H. Strickland, T. Smith, and K. Sun. A vortex model of the darrieus turbine: An analytical and experimental study. Technical Report SAND81-7017, Sandia National Laboratories, 1981.

[5] Jonathan C. Murray and Matthew Barone. The development of cactus, a wind and marine turbine performance simulation code. In *AIAA 49th Aerospace Sciences Meeting*, number 147, 2011.

[6] D. M. Somers. Design and experimental results for the s825 airfoil. Technical report, NREL/SR-500-36346, 2005.

[7] D. M. Somers. Design and experimental results for the s814 airfoil. Technical report, NREL/SR-440-6919, 1997.

[8] Marshall L Buhl. Wt_perf user's guide. *National Wind Technology Center, National Renewable Energy Laboratory, Golden, CO*, 2004.

[9] Brian R. Resor. National rotor testbed requirements. Technical Report SAND2015-9142, 2015.

DISTRIBUTION:

1 MS 0899 Technical Library, 9536 (electronic copy)


Sandia National Laboratories